ROYAL SOCIETY OF CHEMISTRY

PAPER

Check for updates

Towards a higher level of circularity in lithium brine mining: CO_2 absorption in concentrated brines

Nadia C. Zeballos, [ID] [ab] Walter R. Torres [ID] *[a] and Victoria Flexer [ID] *[a]

The transition to sustainable lithium production from brines requires innovations that address chemical consumption, water use, and carbon emissions. This work proposes a novel six-step treatment of real, highly saline lithium-rich brine to simultaneously recover lithium carbonate (Li_2CO_3), co-produce sodium carbonate (Na_2CO_3), and achieve permanent CO_2 storage through mineralization. The strategy integrates five electrochemical steps—employing an anion exchange membrane—with one chemical CO_2 absorption step. Electrolysis initially raises the brine pH to eliminate divalent cations without chemical additives. Subsequent CO_2 sparging in alkaline brines induces Li_2CO_3 and later Na_2CO_3 precipitation. Results demonstrate 78% Li^+ recovery as impure Li_2CO_3 and 71.8% Na^+ recovery as Na_2CO_3. Notably, 205.8 g of CO_2 per litre initial brine were absorbed, of which 189.7 g were permanently stored in solid carbonates. The process minimizes chemical input, reduces reliance on remote chemical delivery, and leverages high brine salinity to enhance CO_2 capture kinetics and electrochemical efficiency. Though not optimized for energy consumption, this proof-of-concept study reveals a circular approach to lithium extraction, integrating critical material recovery with climate-relevant carbon capture. Future improvements could enable direct air capture integration and Li_2CO_3 purification. This study introduces an industrially relevant pathway to reduce the environmental impact of lithium brine mining by turning waste brine constituents into valuable, stable products while closing the carbon cycle through mineralization.

Sustainability spotlight

This work presents a sustainable approach to produce lithium carbonate from brines and simultaneously capture carbon dioxide. The findings contribute to advancing sustainable mining technologies and support progress toward 4 UN Sustainable Development Goals: Affordable and Clean Energy (SDG 7); Industry, Innovation and Infrastructure (SDG 9); Responsible Consumption and Production (SDG 12); and Life on land (SDG 15). Lithium is fundamental for energy transition. It would be an inconsistency if its increased production would be associated with non-sustainable practices. The new brine processing methodology fully avoids the use of soda ash for lithium carbonate precipitation. This is replaced by CO_2 absorption in alkaline media produced *via* water electrolysis. CO_2 is permanently captured and stored in the mineralized products.

1. Introduction

Carbon capture, utilization and storage has a fundamental role in achieving several of the United Nations Sustainable Development Goals.[1] Electrochemical CO_2 capture technologies are attracting increasing attention due to their flexibility and their ability to address decentralized emissions.[2,3] Moreover, they are particularly attractive in locations with high potential for renewable energy generation.[2,4] Most commonly, these CO_2 capture methodologies are based on the trivial capability of electrochemical methods to swing the pH of the CO_2 absorbing solution. The hydration and dehydration equilibrium is used first to capture CO_2, and potentially release it more concentrated in the second stage, if required, by re-acidification. Electrochemically, the pH of the solution can be adjusted without addition of chemicals[2,5] by electrolysis,[6] bipolar membrane electrodialysis,[7–9] reversible redox reactions[10–12] and capacitive deionization.[13] A non-negligible advantage of electrochemical methods is their ability to couple CO_2 capture and utilization. The main challenge of any CO_2 capture technology is high energy consumption, coupled with the still reduced implementation of tax or legislation incentives for the private sector to voluntarily implement such initiatives.[14,15]

The absorption of CO_2 in aqueous solutions and its conversion to bicarbonate anions are favoured thermodynamically. However, at neutral pH, this conversion rate is kinetically slow.[16–18] The kinetics can be considerably accelerated by increasing the pH, the ionic strength of the solution or the

aCentro de Investigación y Desarrollo en Materiales Avanzados y Almacenamiento de Energía de Jujuy-CIDMEJu (CONICET-Universidad Nacional de Jujuy), Av. Martijena S/N, Palpalá, 4612, Argentina. E-mail: wtorres@unju.edu.ar; vflexer@unju.edu.ar

bInstituto Nacional de Tecnología Industrial (INTI) Sede Jujuy, Av. Martijena S/N, Palpalá, 4612, Argentina

temperature. Increasing temperature will however diminish the total amount of inorganic carbon that will be solubilized in aqueous solution. Conversely, increasing the pH will not only increase the kinetics of absorption and conversion but will also radically augment the amount of dissolved total inorganic carbon by over 2 orders of magnitude per pH unit.[2,19] Finally, high salinity brines increase the kinetics of absorption and conversion, are naturally abundant, and aid the implementation of electrochemical technologies, by lowering costs when reducing the electrical resistance of a given media. H_2 production during water electrolysis can partially counterplay the cost of CO_2 capture.[2]

CO_2 capture is only the beginning of the pathway towards sustainability. In order to close the carbon cycle, CO_2 needs to be alternatively utilized or permanently stored. Chemical conversion of CO_2 to products such as alcohols, formic acid or different organics is possible *via* different routes.[7,20,21] The other option is to permanently store CO_2. Gaseous CO_2 can be stored at high pressure in deep geological layers[22] or alternatively by mineralization as solid carbonates.[23–26] The latter is subjected to higher social acceptance as compared to the former, and the storage capacity is potentially unlimited, since it is less restricted by geological conditions in deep layers.[25]

Today, lithium mining from natural brines is performed through a methodology known as the evaporitic technology.[27–29] Briefly, brines are pumped from underground deposits and poured into large, water-proof linen-covered, open-air evaporation ponds where they are let to reside for as long as required until a suitable lithium cation concentration is reached for further processing. This process takes place exclusively in extremely arid regions, such as the Lithium Triangle in South America, the Nevada Dessert or southwestern China, where the weather is sufficiently dry. In addition, large extensions of flat inexpensive land are required to build ponds. After 10–24 months, a large proportion of the more concentrated salts sequentially crystallize in the ponds. At the moment, lithium concentration is high enough for successful crystallization of lithium carbonate and sodium chloride concentration is close to saturation in the concentrated brine.[29]

In the current evaporitic technology, the concentrated brine is first purified to remove borates, magnesium and calcium. Boron is most commonly removed by liquid–liquid extraction in a mixture of kerosene and different alcohols.[29] Magnesium is removed by increasing the pH *via* addition of hydrated lime, while calcium is removed *via* addition of small amounts of soda ash (sodium carbonate).[27,29] In one facility, these three impurities are removed instead by re-dissolving the primary lithium carbonate *via* carbonation and treating the $LiHCO_3$ solution in ion exchange resins that remove said impurities.[30] Lithium carbonate is crystallized *via* addition of soda ash at a temperature close to 90 °C, to take advantage of its inverse solubility.[27,31] Overall, while most concerns about current lithium mining from brines are focused on water issues,[27,28] the large consumption of chemicals in the final processing stage is not to be ignored. In addition to costs and the environmental footprint of the large consumption of chemicals, there are logistical issues associated with the required constant delivery of said

chemicals. Lithium brine mining facilities are exclusively in very remote desertic locations, often on gravel winding roads up the mountains. Railway infrastructure is often not in place in those remotes areas, and lorry transportation of chemicals is sometimes disrupted due to extreme weather conditions, with non-negligible economic impacts.[28]

Herein, we report on a new integrated and intensified chemical process at a proof-of-concept level to simultaneously crystallize lithium carbonate, Li_2CO_3, with the co-production of large amounts of Na_2CO_3, capture CO_2 and permanently store it in said mineralized products. A 6-step processing strategy was developed comprising 5 electrolytic and 1 chemical processing step. The electrolytic steps all comprise a water electrolyser fitted with an anion exchange membrane. Brine is always fed to the cathodic compartment, which is coupled in 4 of 5 electrolytic steps to a side-decanter where CO_2 is continuously sparged. A qualitative–quantitative analysis of all solids and intermediate brines was carried out. The first treatment was successful in the full abatement of divalent cations. The second and third treatments successfully crystallized 78% of the original Li^+ content as primary lithium carbonate (70% purity). The fourth, fifth and sixth steps achieved the crystallization of 71.8% of the original Na^+ content as sodium carbonate. Despite the large depletion of salts, the effluent brine was only reduced by 10% in total dissolved solid content, because the original brine volume was also reduced to 40% of its original volume and the remaining salts were then contained in a much more reduced solution volume. In the overall technology proposal, a total of 205.8 g_{CO_2} L_{brine}^{-1} were captured in both brine and solids, 189.7 g_{CO_2} L_{brine}^{-1} of which are considered to have also been permanently stored in highly stable mineralized products: Li_2CO_3 and Na_2CO_3.

2. Materials and methods

2.1. Experimental setup

A schematic representation of the 6-step brine treatment proposed here is shown in Fig. 1. It comprised 5 electrochemical steps and one pure chemical step (step 4). The first brine processing step, named ELECTROLYSIS E0, is an electrochemical process, carried out to eliminate divalent cations (see Fig. 1, flux diagram on the left, coloured in black). The electrolysis was carried out for 3.5 h at 200 A m^{-2}, according to the initial composition of the brine, for the successful elimination of divalent cations. The second and third brine processing steps, named ELECTROLYSIS E1.1, and E1.2, respectively, were accomplished to alkalinize the brine, to favour absorption of CO_2, and trigger the crystallization of lithium as lithium carbonate (Fig. 1, flux diagram on the left, coloured in blue). The electrolysis was carried out at alternatively 300 and 350 A m^{-2}. ELECTROLYSIS E1.1 was carried out until the large amount of solids accumulated in the reactor made solution recirculation difficult. ELECTROLYSIS E1.2 was carried out until the amount of solids did not seem to increase any further (see Fig. S1 in the SI).

The fourth brine processing step, named CHEMICAL C2, is a chemical absorption step of CO_2. Technical grade CO_2 was
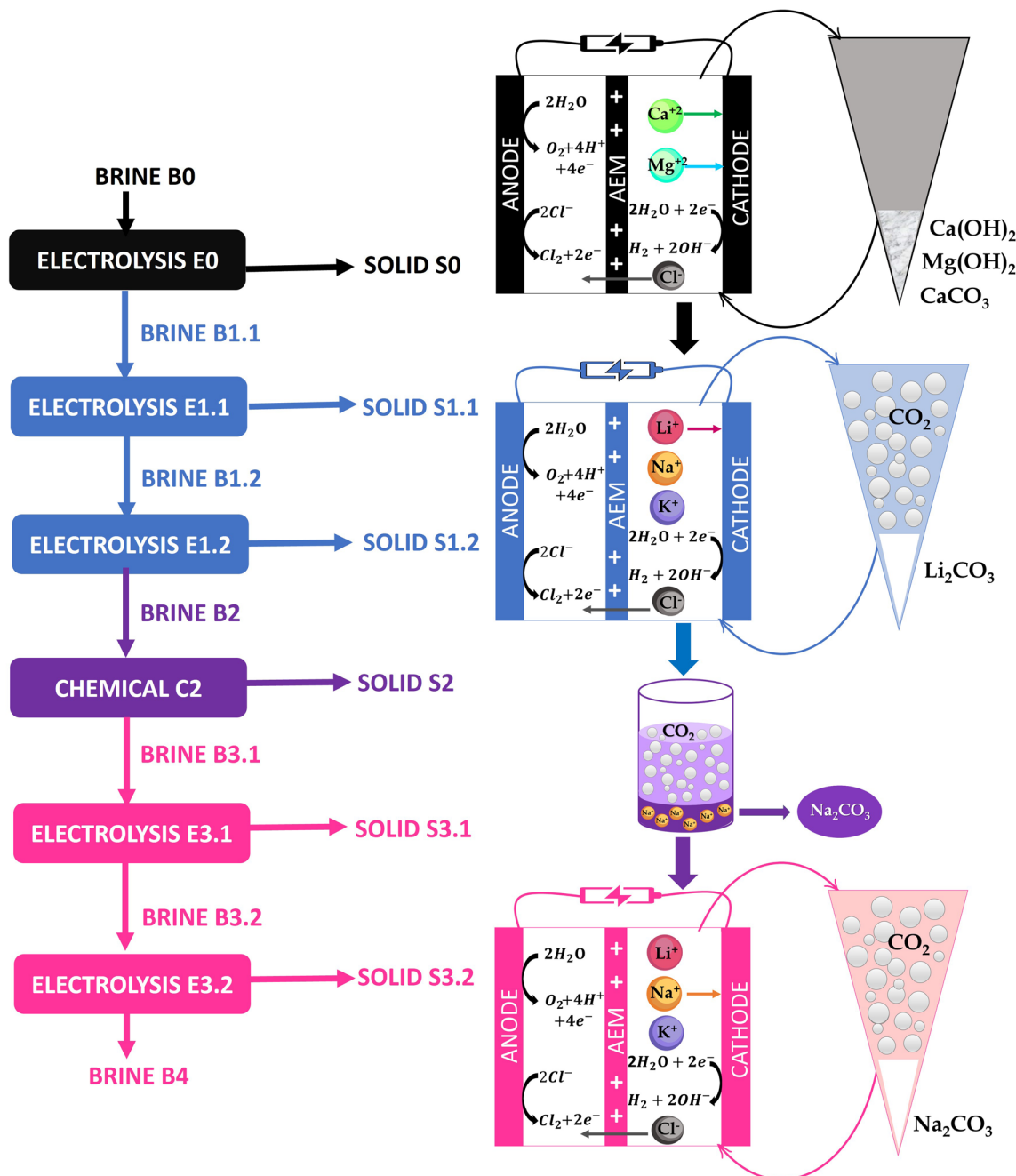
Fig. 1 Representative scheme of methodology applied in anhydrous carbon absorption from brines. In black is shown the process not-involving CO_2 absorption. In blue is shown the methodology to co-obtain lithium salts. In purple is shown the chemical process for obtaining sodium crystals. In pink is shown the electrochemical process to co-obtain sodium salts.

sparged in the brine in an open vessel for 14.0 minutes at a flow rate of 176 mL min^{-1}. This step triggered the crystallization of sodium carbonate (Fig. 1, flux diagram on the left, in purple). The fifth and sixth brine processing steps were methodologically similar to the second and third processing steps, although sodium carbonate was the main crystallized compound.

At the end of each of the 6 steps, the suspension in the cathodic compartment and the connected crystallization vessel was filtered, and the solids were dried at 100 °C for chemical analysis. An aliquot of the obtained supernatant was separated

for analysis, and the remaining brine was further processed, as indicated in Fig. 1. Experimental conditions for all 6 steps are detailed in Table 1.

2.1.1. Electrochemical setup. A two-compartment electrochemical reactor manufactured in-house with similar specifications as described in Desloover *et al.* was used in all electrochemical experiments.[32] Two acrylic frames with internal dimensions of $5 \times 20 \times 2$ cm, separated by an anion exchange membrane (AEM, model AMI-7001CR, Membrane International Inc., USA), were assembled together and fixed, yielding an

Table 1 Detail experimental conditions for the six process steps

Step	Total circulated charge (C)	Average current applied (A)	Maximum current applied (A)	Experiment duration (h)	Mass of CO_2 bubbled[a] (kg)	Initial brine volume (L)	Final brine volume (L)
E0	26 910	2.10	4.26	3.55	0	2.00	2.00
E1.1	274 095	2.99	3.51	25.48	0.448	2.00	1.75
E1.2	266 730	3.96	4.00	18.72	0.330	1.75	1.55
C2	0	0.00	0.00	8.33	0.147	1.55	1.40
E3.1	136 714	2.02	2.02	18.80	0.331	1.40	1.00
E3.2	126 048	2.02	2.02	17.33	0.305	1.00	0.80

[a] Calculated at 20 °C and 0.92 bar.

internal volume of 200 mL for both anodic and cathodic compartments. The electrodes were separated about 2 mm with a plastic mesh to avoid direct contact with the membrane. The anode was a titanium mesh covered with a mixture of iridium and titanium oxides, (IrO_2/TiO_2: 65/35%; dimensions: 4.8 cm × 19.8 cm × 1 mm, Magneto Special Anodes), and the cathode was a 316 stainless-steel mesh. Experiments were run at a constant current by using a UNI-T Instrument DC/DC regulated power supply. Fig. S2 shows a picture of this setup. The properties and characteristics of anionic membrane are listed in Table S1. Membranes were previously immersed in 5% NaCl overnight to allow their hydration and expansion. Before usage, they were washed with ultra-pure water and kept in 5% NaCl solution when not in use.

The anodic compartment was connected to a 2.0 L plastic drum, whilst the cathodic compartment was connected to a 2.0 L Schott bottle serving as a decanter. Initially, the volume of brine treated was 2.00 L (for Electrolysis E0 and E1.1). For Electrolysis E1.2, Chemical C2, Electrolysis E3.1, and E3.2, initial volumes were 1.75 L, 1.55 L, 1.40 L, and 1.00 L respectively. The final volume of brine B4 of the overall process was 0.80 L. Brines and anolyte were continuously recirculated in electrochemical steps with the aid of a peristaltic pump (6 L h^{-1}, PC28 APEMA, Argentina) with the aim of forcing mass transport. For the chemical step, bubbling also facilitates the stirring phenomenon. To avoid chlorine production in the anodic compartment, a carbonate–bicarbonate buffer was used as the anolyte (2 M, pH 10, industrial grade).[33]

2.2. Initial brine

The departing brine sample, termed Brine B0, was a generous sample from a lithium mining plant in the Northwest of Argentina, a de-identified site. The composition of this brine is listed in Table 2. This is not a native brine sample. The native brine contained a much reduced Li^+ content, in the order of 600–900 ppm Li^+. Brine B0 was obtained after the native brine was left to rest for approximately a year in a series of solar evaporation ponds, which allowed for the loss of water from the original brine by natural evaporation, producing an increase in Li^+ concentration, and the crystallization of a portion of the most concentrated salts, such as NaCl and KCl. Hydrated lime was added at some point before collection to eliminate a large portion of Mg^{2+} from the concentrated brine (which explains the high pH of Brine B0). This type of concentrated brine is representative of those generated in various lithium mining operations in countries such as Chile, Argentina, the United States, and China.

2.3. Analysis

X-ray diffraction (XRD) patterns were measured to characterize chemical structures. An X-ray powder Rigaku MiniFlex diffractometer (45 kV and 30 mA) with a copper anode and a curved graphite monochromator was employed. XRD patterns were recorded over a 2θ range from 4 to 90° with a step of 0.02°. The results were compared with different lithium reference patterns to assign the main chemical structure and impurities.

Scanning electron micrographs were determined to evaluate the particle size, morphology, and surface appearance at 3 kV acceleration voltage, at a working distance between 9–10 mm, with 40 nm of gold covering, and using a secondary electron detector (SEM, Carl Zeiss, Jena, Germany, EVO MA10 model, equipped with a W filament).

Measurements to assess the chemical composition of brines and solids were conducted using an Agilent 5800 inductively coupled plasma-optical emission spectrometer (ICP-OES). Each analysis was repeated three times, and the obtained values correspond to the mean value. Solids were dissolved in 5%

Table 2 Composition of the departing brine sample

Brine	g L^{-1}								
	Li$^+$	Na$^+$	K$^+$	Ca^{2+}	Mg^{2+}	Cl$^-$	SO$_4^{-2}$	B	CO$_3^{-2}$
B0	6.0 ± 0.3	112 ± 4	59 ± 2	0.043 ± 0.003	0.069 ± 0.002	190 ± 7	0.55 ± 0.07	3.47 ± 0.15	16.8 ± 0.5

Table 3 LCIA results for the climate change indicator for selected energy sources

Energy source	CO$_2$ equivalent emissions per kW h gCO$_2$ equivalent^{-1}
Natural gas (without CO$_2$ capture)	486
Oil (without CO$_2$ capture)	840
Concentrated solar power (tower and trough)	28
Photovoltaics (thin film and crystallized Si)	43
Wind	13

HNO$_3$ to assess their composition. Chloride and carbonate anions were determined by volumetric titration.

Conductivity was determined in a sample diluted 1 : 500 in the solution of interest with a conductivity probe (HI763063 probe and HI99301 controller, HANNA). Brine density was determined by measuring ten times the weight of 1.000 mL of sample and averaging the results. The pH was determined by an acid–base titration. 0.10 mL samples were taken to measure the total dissolved solids (TDS).

2.4. Calculations

The relative volume changes in Fig. 3 refer to the volume change in one single processing step (*e.g.* ΔV/Vi for E2 is equal to the volume difference achieved between the end and start of electrolysis E2, divided the initial brine volume entering E2).

The amount of sequestered CO$_2$ in these experiments was calculated assuming that the difference in Li$^+$ and Na$^+$ contents between different brines and B0 corresponds to crystallized Li$_2$CO$_3$ and Na$_2$CO$_3$, respectively. K$_2$CO$_3$ was not considered since it was not observed in the diffractograms. The missing amounts of Li$^+$ and Na$^+$ were converted to moles. The number of moles of the corresponding carbonates (in moles) is half the number of moles of the corresponding cations. Finally, the mass of carbonate was converted to CO$_2$ (factor 60/44) and divided by 2 so that the final result would correspond to 1 L of initial brine fed to the first electrolytic step (ELECTROLYSIS E0).

CO$_2$ emissions considering different energy sources were calculated using data from Life Cycle Impact Assessment (LCIA) of Electricity Generation Options[34] summarized in Table 3.

3. Results and discussion

3.1. Proposed brine processing

3.1.1. First set of electrolytic steps. The first processing step (B0 is the initial composition and B1.1 is the final composition) was devised to increase the brine pH with the aim of causing the abatement of the small amount of divalent cations present in the as-received brine (see Fig. 1, top left). Electrolysis E0 effectively produces the full abatement of Mg^{2+} and Ca^{2+}. After filtering the obtained suspension, both Mg^{2+} and Ca^{2+} were below the ICP detection limit in the supernatant. Cation and anion composition, together with physical–chemical parameters of brines, after different processing steps are shown in Fig. 2 and 3. The other brine components remained almost constant after Electrolysis E0. The slight increase in concentration is explained by water splitting at the electrode surface.

In the second processing step (B1.1 is the initial composition and B2.1 is the final composition), water electrolysis was carried out with concomitant CO$_2$ sparging to favour CO$_2$ absorption. The sequestration of CO$_2$ in alkaline solutions was favoured due to the equilibria system depending on the pH of the solution. At high pH, the equilibrium is displaced to carbonate formation (eqn (1)–(3)).[16–18] If lithium and/or sodium concentrations are high enough, precipitation of the corresponding carbonates can be achieved (eqn (4) and (5)), and the equilibria in eqn (1)–(3) are further driven to product formation, *e.g.* absorption of larger absolute amounts of CO$_2$.[19,35,36] At intermediate pH values, bicarbonate is the main C species and provided that Na$^+$ concentration is high enough that NaHCO$_3$ can be obtained (eqn (6)).[9,36]

$$2H_2O + 2e^- \rightleftharpoons 2OH^- + H_2 \tag{1}$$

$$OH^- + CO_2 \rightleftharpoons HCO_3^- \tag{2}$$

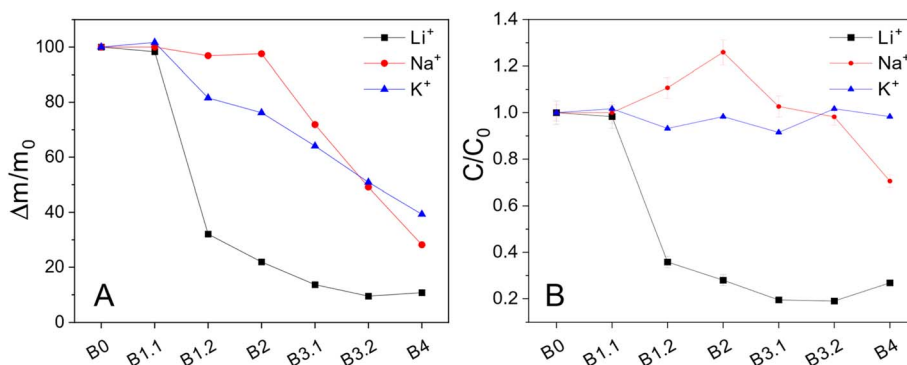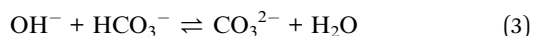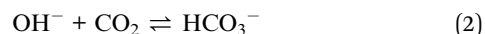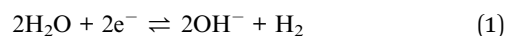$$OH^- + HCO_3^- \rightleftharpoons CO_3^{2-} + H_2O \tag{3}$$

Fig. 2 (A) Percentage of initial amount of the respective cations remaining in the processed brines. (B) Concentrations (*C*) relative to the initial value (*C*$_0$) of Li$^+$, Na$^+$, and K$^+$ in brines in different steps.

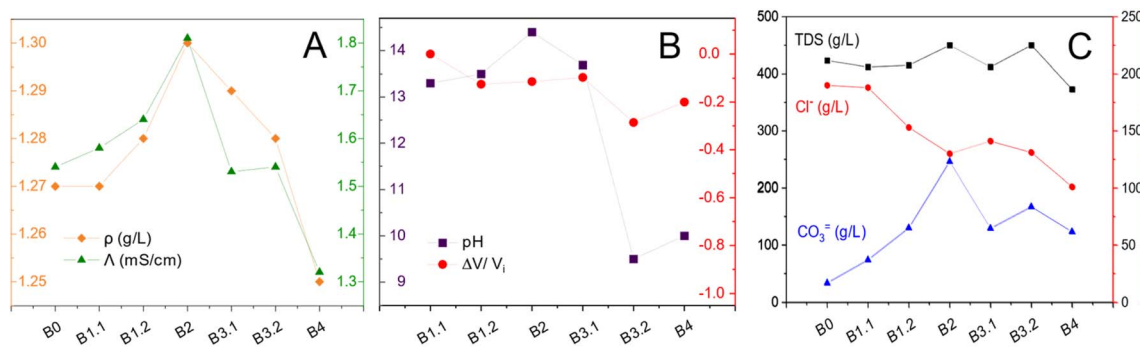© 2025 The Author(s). Published by the Royal Society of Chemistry

Fig. 3 Physical and chemical parameters of different brines. (A) Density (direct measurement) and conductivity (1 : 500 dilution). (B) pH and relative volume decrease. (C) Total dissolved solids (TDS), chloride and carbonate concentrations.
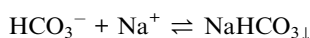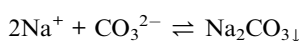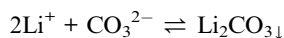
$$2Li^+ + CO_3^{2-} \rightleftharpoons Li_2CO_{3\downarrow} \tag{4}$$

$$2Na^+ + CO_3^{2-} \rightleftharpoons Na_2CO_{3\downarrow} \tag{5}$$

$$HCO_3^- + Na^+ \rightleftharpoons NaHCO_{3\downarrow} \tag{6}$$

Fig. 2 indicates that Electrolysis E1 produces a marked decrease in the C/C_0 ratio for Li^+, falling to 0.321 times its initial value. This behaviour indicates that Electrolysis E1.1 effectively operates as a lithium extraction process, in which Li^+ removal occurs within the decanter attached to the cathodic compartment. Water electrolysis generates OH^-, raising the pH above 13–14 and allowing the formation of carbonate anions from dissolved CO_2. These react *in situ* with Li^+ to form lithium carbonate (Li_2CO_3). The anionic membrane (AEM in Fig. 1) serves to separate the anolyte and catholyte, avoiding H^+ from the anode reaching the cathode and allowing the control of the pH. The AEM is not selective to different anions, and chloride,

sulphates, borates and hydroxyl species can all migrate to maintain electroneutrality in both compartments. Fig. 3C suggests that chloride species are the main charge carriers. In contrast, during Electrolysis E1, Na^+ and K^+ cations maintain C/C_0 values close to 1, indicating that they mostly remain in solution (see the discussion on solid compositions below). After filtration of solid S1.1, Electrolysis E1.2 was started following the same procedure as before. A new solid S1.2 was obtained. Fig. 2 shows that the Li^+ content can further decrease, although at this step, only 10% of the original Li^+ content was removed from the brine (*vs.* 67% during Electrolysis E1.1).

Fig. 4 shows the diffractograms of all solids obtained throughout processing. The X-ray diffractogram of S0 indicates it is mostly composed of NaCl and KCl. While no other diffraction peaks are observed, elemental analysis also shows the presence of Li^+, Mg^{2+} and Ca^{2+}, determined as 0.0114 ± 0.0007, 0.024 ± 0.001, and 0.048 ± 0.003 g per gram of solid,
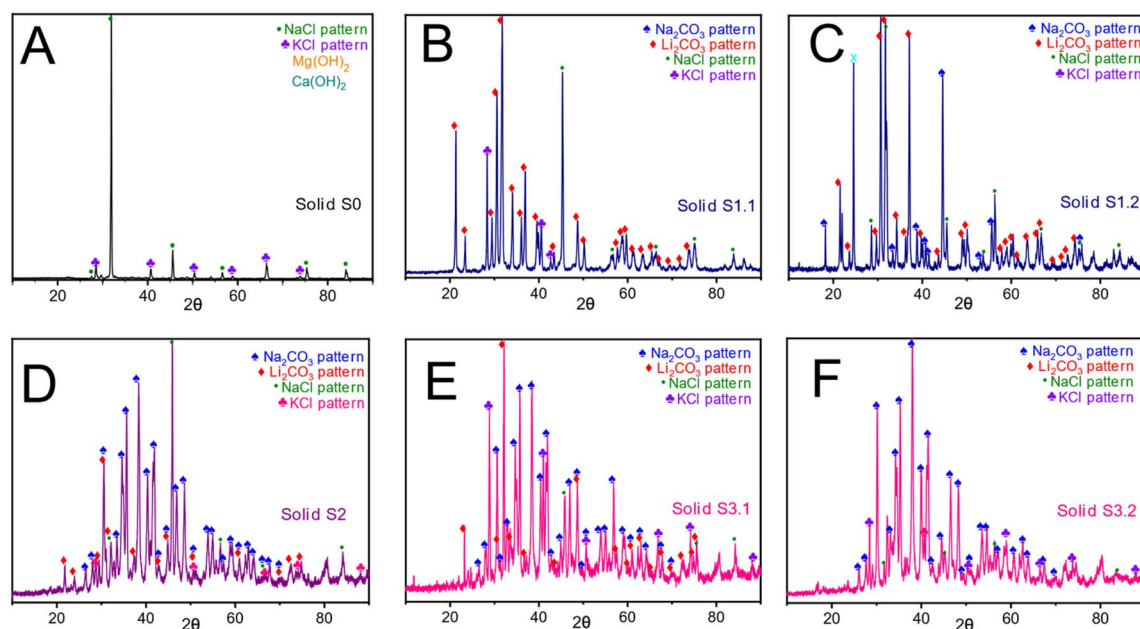

Fig. 4 X-ray diffractograms of the different solids obtained. Different diffraction peaks are assigned to reference diffraction patterns as indicated in each panel. Panels A–F show the X-ray diffractograms of solids S0, S1.1., S1.2, S2, S3.1 and S3.2, respectively.
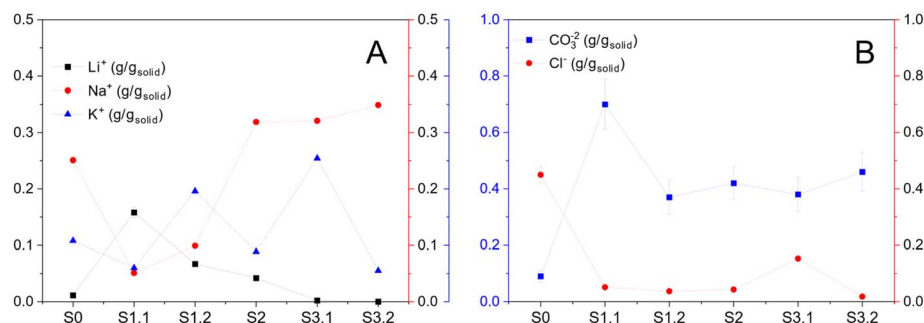
Fig. 5 Composition of solids. (A) Li^+, Na^+, and K^+. (B) Carbonate and chloride.

respectively, *e.g.* with considerably lower compositions as compared to both Na^+ and K^+ (see Fig. 5). The abatement of Mg^{2+} and Ca^{2+} cations is associated with the *in situ* production of hydroxyl anions causing the precipitation of $Mg(OH)_2$, $Ca(OH)_2$ and $CaCO_3$ following the reactions in eqn (7)–(9).

$$Mg^{2+} + 2OH^- \rightarrow Mg(OH)_2\downarrow \qquad (7)$$

$$Ca^{2+} + 2OH^- \rightarrow Ca(OH)_2\downarrow \qquad (8)$$

$$Ca^{2+} + CO_32- \rightarrow CaCO_3\downarrow \qquad (9)$$

$Mg(OH)_2$ is well known for precipitating with very small particles,[37,38] below 500 nm average diameter, and thus adsorbing other ions and entrapping relatively large brine amounts, which upon drying, explain the NaCl and KCl diffraction peaks in S0.

The X-ray diffractogram of S1.1 shows distinctive peaks identified as Li_2CO_3, with peaks of lower intensity assigned to NaCl and KCl. The corresponding diffractogram of S1.2 also shows peaks for Li_2CO_3, with lower intensity peaks assigned to NaCl and Na_2CO_3. The solid purity values were calculated as 71% and 36% in Li_2CO_3 for S1.1 and S1.2, respectively. The quantitative solid analysis shown in Fig. 5 is in good agreement with the X-ray diffractograms. Solid purification was beyond the scope of this work. Impurities identified just above are highly water soluble (NaCl, KCl and Na_2CO_3). Li_2CO_3 shows an inverse solubility with temperature,[31] hence solid washing with pure water at approximately 95 °C is suggested as the best alternative to purify both S1.1 and S1.2 while minimizing Li_2CO_3 loss. Countercurrent washing should minimize freshwater requirements for solid washing.

This proposal replaces the cost and the logistical hurdles of shipping large amounts of chemical reagents to remote mining locations, while CO_2 is captured and permanently stored (see Section 3.5). The percentage of Li^+ recovery from the brine originally fed to the system is similar to current practice *via* crystallization with soda ash, and the amount of Li^+ remaining in brine is due to the relatively large solubility of Li_2CO_3[29] of 13.0 g_{kgH_2O} at 25 °C.

3.1.2.   Chemical processing. In the fourth processing step (departing from B2 to reach B3.1) the system passes from an electrochemical to a chemical step where sodium is partially removed from the brine. During the chemical treatment,

a decrease in both Na^+ and K^+ contents in the brine (Fig. 2A) is observed, accompanied by a plateau in Cl^- levels and a drop in CO_32-. This behaviour is interpreted as a consequence of CO_2 absorption in the brine, which, under alkaline conditions, favours the formation of carbonate species (eqn (2) and (3)) that react with Na^+ to precipitate as Na_2CO_3 (eqn (5)). The maximum CO_3^{2-} is reached at the end of the third electrolytic step. The subsequent chemical step produces a drop in the CO_3^{2-} concentration that agrees with the decrease in Na^+ concentration, suggesting effective recovery of Na^+ in the form of a solid salt. The crystallization of Na_2CO_3 seems to take place only when the Li^+ concentration has been largely depleted, in agreement with the much higher solubility value of Na_2CO_3, as compared to Li_2CO (2.9 *vs.* 0.18 mol kg_{H2O}, respectively, in pure water at 25 °C).[31] Qualitatively, the kinetics of crystallization of Li_2CO_3 seem to be faster than those of Na_2CO_3.

The collected solid S2 shows sharp peaks of Na_2CO_3 according to XRD analysis, with concurrent presence, albeit at a lower intensity, of Li_2CO_3, KCl and NaCl. The XRD data are again in good agreement with the composition analysis which indicates that Na^+ and CO_3^{2-} are the major species, with a calculated solid purity in Na_2CO_3 of 68% (previous to any purification step). A pH of 9.5 had been reached at the moment when solid S2 was filtered (Fig. 3B). Knowing that continuing with CO_2 sparging would result in a further decrease in pH and that this would favour the presence of bicarbonate anions over carbonate (eqn (2)), the decision to further increase the pH electrochemically was taken.

At 1.23 mol kg_{H2O} *vs.* 2.9 mol kg_{H2O}, the solubility in pure water of $NaHCO_3$ is slightly lower than that of Na_2CO_3.[31] Targeting the crystallization of $NaHCO_3$ instead of Na_2CO_3 is a plausible alternative yet to be tested. From the perspective of CO_2 capture and storage, $NaHCO_3$ can store twice the amount of CO_2 as compared to Na_2CO_3. However, from the perspective of brine desalination, the crystallization of Na_2CO_3 deprives the brine from twice the amount of Na^+, as compared to $NaHCO_3$.

3.1.3.   Second set of electrolysis. Electrolysis E3.1 was started to further raise the brine pH and increase the CO_2 fixation. For the second time during processing, a large proportion of Na^+ content in the brine is crystallized (B3.1 to B3.2), evidenced by a drop in both Na^+ and K^+ contents, with the content dropping by 22.1 and 13.1% of their original content, and a minor

drop in the Li^+ concentration of 4.4% of its original content (Fig. 2A). The X-ray diffractogram shows that solid S3.1 is mostly composed of Na_2CO_3, with lower intensity peaks corresponding to Li_2CO_3, KCl and NaCl, in agreement with data in Fig. 5. The continuous observed precipitation of Li_2CO_3 is attributed to the brine volume decrease, which allows for Li_2CO_3 to reach saturation again triggering its crystallization. Conversely, the presence of both KCl and NaCl is attributed to ion adsorption in the large amount of crystallized solid, since both species are still far from their solubility values. In this proof-of-concept experimental setup, Electrolysis E3.1 had to be stopped because of the accumulation of considerable solid amounts within the electrochemical reactor (no in-line filtering was used).

After filtration of the suspension, further electrolytic treatment coupled to CO_2 sparging was started, following exactly the same procedure, and this final treatment was named Electrolysis E3.2. Both Na^+ and K^+ contents continued to decrease, now with content drops of 20.9, 11.5, and 1.2% of the respective original contents of Na^+, K^+ and Li^+ (Fig. 2A). The X-ray diffraction pattern of solid S3.2 (Fig. 5G). is quite similar to that of the solid obtained during the previous step, Electrolysis E3.1, except that no peaks are observed for Li_2CO_3, while those of NaCl are of much lower intensity as in solid S3.1. The elemental content of solid S3.2 (Fig. 4) is also in good agreement with its diffraction pattern. Overall, ELECTROLYSIS E3.1 and E3.2 can be considered the same processing step. Changes observed in brine composition and physico-chemical parameters follow the same trends, while the two obtained solids are very similar. In a hypothetical larger scale application with on-line filtering of solids, there would be no need to interrupt the processing, as performed here.

Overall, after the 6-step processing strategy, the net diminution in these cations in brines was 1.514, 6.994, and 1.882 moles, corresponding to 87.6%, 71.9% and 63.4% of the initial Li^+, Na^+ and K^+ contents, respectively, in addition to 100% removal of Mg^{2+} and Ca^{2+}. These changes in cation content occur along with the production of Li_2CO_3 and Na_2CO_3, that is why we considered the proposed strategy as a circular economy approach, since it produces two different products and minimizes liquid waste, in addition to capturing and storing CO_2.

3.2. Further brine analysis

Because of the extremely high salinity, density values for all these brines are above 1.25 g cm^{-3}. Brine conductivity was also very high, and therefore only the conductivity values of 1 : 500 dilutions could be measured. Brine density, conductivity, pH, volume changes, TDS, and chloride and carbonate contents are depicted in Fig. 3. The brine density remains unchanged in the short ELECTROLYSIS E0 step, while its conductivity increases. Both brine density and conductivity increase during the much longer ELECTROLYSIS E1.1 and 1.2 steps. The increase in conductivity is undoubtedly explained by the increase in pH, due to the *in situ* formation of hydroxyl anions, whose molar conductivity is known to be higher than that of the chloride anions that are replaced during electrolysis.[39] The maximum value reached for brine density in B2 correlates with the

concentration of Na^+ in brine, in agreement with its behaviour shown in Fig. 2. While the Na^+ content is almost the same as that in the starting brine, the concentration increases due to the brine volume decrease (explained below). In the chemical step (B2 to B3.1), a marked drop in brine density is observed, explained by the sharp decrease in pH. Following the same reasoning as above, the decrease in brine density is associated with the large precipitation of sodium salts. In the last two electrochemical steps (B3.1 to B4), the conductivity and density of brine decrease due to the precipitation of large amounts of salt, mostly sodium carbonate, as shown in Fig. 2.

It is observed that the brine volume is reduced during ELECTROLYSIS E1.1, 1.2, 3.1 and 3.2. This is explained to a large extent by electro-osmotic effects (anions are mostly transferred across the ionic exchange membrane in a hydrated form),[33] by water electrolysis at the cathode (about 250 g H_2O in total), and likely due to poor filtration of large amounts of solids. The latter could be reduced on a laboratory scale with vacuum filtration and/or centrifugation, although it was preferred to stick to simple filtration steps to resemble more closely to a potential industrial application. The duration of the electrolytic steps was far from being optimized. Electrolysis and CO_2 absorption were let to run, while the amount of crystallized solids was observed to increase, although this was only a qualitative appreciation. Shorter electrolytic treatments would have resulted in lesser volume changes. Indeed, only in the short ELECTROLYSIS E0 step, the change in the volume is negligible.

Anions' concentrations are shown in Fig. 3C. Chloride composition fell in all electrolytic steps due to the migration of these anions from the catholyte compartment to the anolyte through the anion exchange membrane. While chloride concentration fell only to half of the initial concentration, since the brine volume was reduced by over half of the initial value, and the total content of chlorides was reduced in 8.44 moles of Cl^- migrated, corresponding to 78.7% of the total initial chloride content in B0. Carbonate anions' concentration increased during ELECTROLYSIS E0, E1.1 and E1.2. While no CO_2 was sparged during ELECTROLYSIS E0, the increase in carbonate concentration is explained by direct absorption of CO_2 in air (the decanter was open to the atmosphere). This is interesting because it opens up the possibility to studying direct CO_2 capture from air, although this is beyond the scope of this work. However, this is the most interesting possibility both in terms of reducing operation costs and sustainability. For the successive steps, with large Li^+ and Na^+ concentrations to be crystallized, direct capture from air would entail longer residence times, since the kinetics of CO_2 absorption would be slower considering the reduced CO_2 concentration in air (at about 400 ppm, more reduced at high altitudes due to lower atmospheric pressure). The energy consumption would also be reduced, although the 5 electrolytic steps are part of the overall process, the reduction in energy consumption could be rather small considering that electrolytic steps often take the largest share of energy consumption in the overall technology (see Section 3.4).[39]

The increase in carbonate concentration was even faster when CO_2 was sparged (it should also be considered that part of

the captured CO_2 was removed as the solids were separated from the suspension). Carbonate decreases sharply after the chemical step, which is easily explained by the decrease in pH to about 9.0 shifting the equilibrium to bicarbonate species (eqn (2)). Carbonate concentration never reached the maximum value again, despite continuous electrolysis and sparging, since during ELECTROLYSIS E3.1 and 3.2 it was kept at lower values than before (never higher than 11, as compared to higher than 13 in ELECTROLYSIS E1.1 and E1.2).

Fig. 3C shows that the TDS value remains at extreme salinity values close to 400 g L^{-1} during all processing, falling to 370 g L^{-1} by the end of the brine processing. At first glance, this might seem a very poor performance in terms of brine desalination. A closer look indicates that the initial brine volume was reduced by 60% (Fig. 3B), *e.g.* while the TDS value was only reduced in about 10%, the amount of salts that was not removed from the initial brine is now present in a much reduced brine volume. In turn, it should also be noted that hydroxyl anions present in brine B0 at a concentration close to 0.5 M decrease in to about 10^{-4} M after the first three electrolytic steps. Hydroxyl anions are mostly replaced by carbonate anions to balance charge, and these add a higher value to the TDS (34 g for 2 moles of hydroxyl *vs.* 60 g for 1 mole of carbonate, accounting for the same amount of negative charges).

The water contained in the initial brine is not irreversibly lost entirely. H_2 and O_2 produced at the electrodes should certainly be captured, particularly the former, and re-used as a fuel, which would regenerate water. Water migration across the anion exchange membrane could be reduced first by reducing the duration of the electrolysis, which is of utmost importance also in terms of energy consumption. Second, electro-osmotic effects could be reduced by using a membrane with lower water permeability.

In the case of S2, Na_2CO_3 is the key product of the chemical step. In the same way, it was observed that there is a non-negligible coprecipitation on Li_2CO_3 for S2 and adsorption of brine, as shown by the peak of NaCl at $2\theta = 45°$. The attenuation of the Li_2CO_3 peaks in these samples reinforces the idea that the system allows for sequential and selective recovery of carbonates, first precipitating Li_2CO_3 and then Na_2CO_3 under controlled conditions. These results suggest that, even without purification steps, it is possible to guide the process toward obtaining differentiated products of interest, which constitutes a significant advantage for the development of direct lithium extraction (DLE) technologies with stepwise cation separation. For the solids obtained from the last electrochemical step, S3.1 and S3.2, they are similar to S2. It is important to note that none of the solids were washed after recovery, implying that the crystallographic profiles include both precipitation products and species possibly adsorbed from the residual brine.

3.3. Scanning electron microscopy analysis

In Fig. 6, scanning electron micrographs show the shape and size of the obtained solids. For comparison, the micrographs for analytical grade commercial samples of Li_2CO_3, Na_2CO_3 and KCl are also shown. Fig. S3 in SI shows the micrographs of analytical grade commercial samples of $NaHCO_3$ and NaCl. Solids S1.1 and S1.2 were previously identified *via* ICP-OES and X-ray diffraction analysis as composed mostly of Li_2CO_3. The latter shows crystals with homogeneous prismatic shapes, while the former also depicts prismatic shapes. These shapes are related to the commercial sample; however, they are much thinner than the commercial samples. The crystals obtained here are also of a more reduced size, in agreement with much lower purity as compared to an analytical grade sample: here,
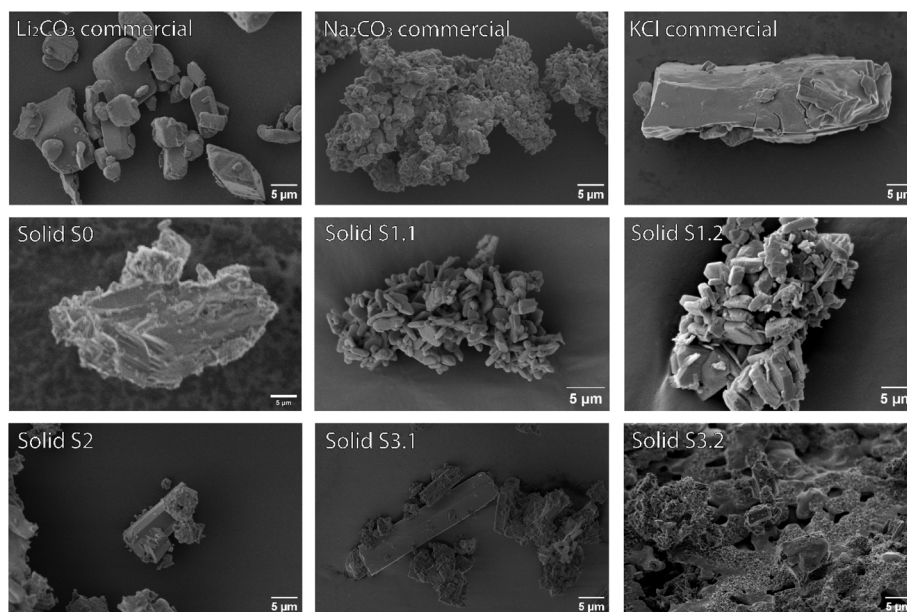

Fig. 6 SEM micrographs of the different obtained solids and commercial pure samples of Li_2CO_3, Na_2CO_3 and KCl, as indicated in each panel.

sizes range from 2 to 5 μm *vs.* prisms starting at 5 μm, with a larger proportion of ∼15 μm for the commercial sample.

None of the three other solids which were identified as being composed mostly of Na_2CO_3 bear a close resemblance to the Na_2CO_3 commercial sample analysed here. The latter consists of agglomerated small crystals, a mixture of prismatic and platelet shapes. In turn, solids S2 and S3.1 are both mostly prismatic. Surprisingly, the size of the crystals obtained for S2 and S3.1 are considerably larger than those of commercial Na_2CO_3, with the sample obtained during the ELECTROLYSIS E3.1 step being even larger than that obtained during CHEMICAL C2. It could actually be argued that these crystals have a mixed shape between Na_2CO_3 and KCl, which is in agreement with the chemical composition (Fig. 4). Finally, the last solid, S3.2, shows smaller size crystals, not resembling much of any of the pure samples analysed here.

3.4. Electrolytic energy consumption

Considering that electrolysis is an energy intensive process, the energy consumption was calculated only for the electrolytic steps. Fluid pumping and CO_2 sparging were not considered in the energy calculation. The electrolytic energy consumption, U_{EC}, was calculated as follows:

$$U_{EC} = \int_0^t E \cdot i \cdot \mathrm{d}t \tag{10}$$

where E is the voltage, i the applied current, and t is the duration of a given electrolytic step.

Fig. 7A presents the energy consumption, expressed in W h L^{-1} of treated brine. Electrolysis E0 requires the lowest energy consumption due to a low composition in divalent cations. Electrolysis E1.1 and E1.2 show the highest energy consumption above 200 W h L^{-1}, which reflects the intensity of electrolysis in these steps. In turn, Electrolysis 3.1 and 3.2 show a more moderate energy consumption (below 150 W h L^{-1}), which suggests an improvement in the CO_2 fixation process efficiency. The chemical step C2, without applied current, showed zero energy consumption, as expected. This proposal was studied here at the proof-of-concept level, and the energy consumption was not optimized. It is believed that the energy

consumption could be considerably decreased from the values calculated here.

3.5. CO₂ capture and storage

CO_2 was absorbed in both brine and solids. Fig. 8A shows the amount of CO_2 absorbed at each of the 6 steps of the process in both brine and solids. The amount of CO_2 absorbed in brine is actually a cumulative value including the amounts absorbed in previous steps. Conversely, since solids are filtered at the end of each step, the CO_2 absorbed amount corresponds solely to the indicated step. For ELECTROLYSIS E0, it should be recalled that CO_2 absorbed is directly captured from air. For ELECTROLYSIS E1.1 and 1.2, the solids retain lower quantities of CO_2 than brine. However, CO_2 captured in solids is known to be permanently stored, while the amount captured in brines could potentially be released depending on brine conditioning, storage or re-injection. During CHEMICAL C2, ELECTROLYSIS E3.1 and ELECTROLYSIS E3.2, the amount of CO_2 captured in solids increases considerably, which is ascribed to the start of the massive crystallization of Na_2CO_3 and the original larger content of Na^+ in brine as compared to Li^+.

Fig. 8B shows the total amount of CO_2 absorbed in the two solid species, Li_2CO_3, Na_2CO_3, and brine. It is interesting to note that if the processing would be interrupted without completion of the 6 steps, the amount of absorbed CO_2 in the solids would be lower than that indicated in Fig. 8B, since a lesser amount of solid would have been recovered. However, Fig. 8A indicates that a higher amount of CO_2 would have been captured in brine. This is explained by both the decreased CO_3^{2-} concentration in brines, as well as the decreasing brine volume as the processing continued (see above). CO_2 permanent storage is a more sustainable solution than an intermediate solution where the fate of capture CO_2 is yet to be determined (capture in brine). In addition, while Na_2CO_3 has a considerably lower market value as compared to Li_2CO_3, it is still a commodity with extremely versatile applications that will find buyers, increasing the revenue of the process.

The partial cumulative plot illustrates the sequestration pathway of CO_2 across two distinct phases: dissolution in brines and mineralization in solid carbonates. A fraction of unreacted CO_2 dissolves in brines, accumulating as aqueous carbonate species. In the initial process steps (ELECTROLYSIS E1.1 and E1.2), lithium carbonate precipitation acts as the dominant mechanism for CO_2 storage. Here, CO_2 is rapidly incorporated into crystalline lithium carbonate solid. During these lithium-recovery focused steps, maximum CO_2 is accumulated in the brine. Beyond these initial steps, sodium carbonate emerges as the primary mineralization product. The continued precipitation of sodium carbonate sustains and accounts for 86.8% of the total amount of mineralized CO_2. The formation of Li_2CO_3 occurs to a lesser extent, although its presence is technologically of utmost importance for the fabrication of rechargeable lithium ion batteries. The first two processing steps demonstrate that selective lithium capture is feasible without the need for additional chemical reagents, solely through electrochemical control of the environment, nucleating conditions, pH
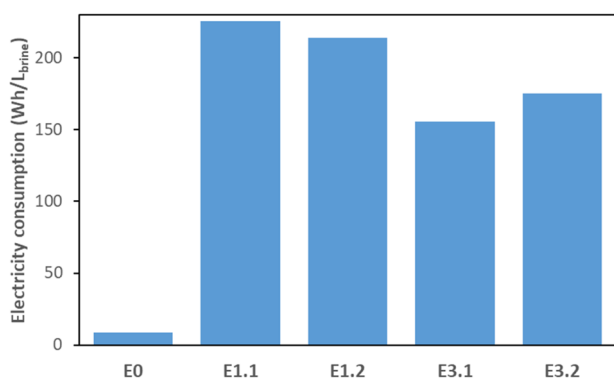

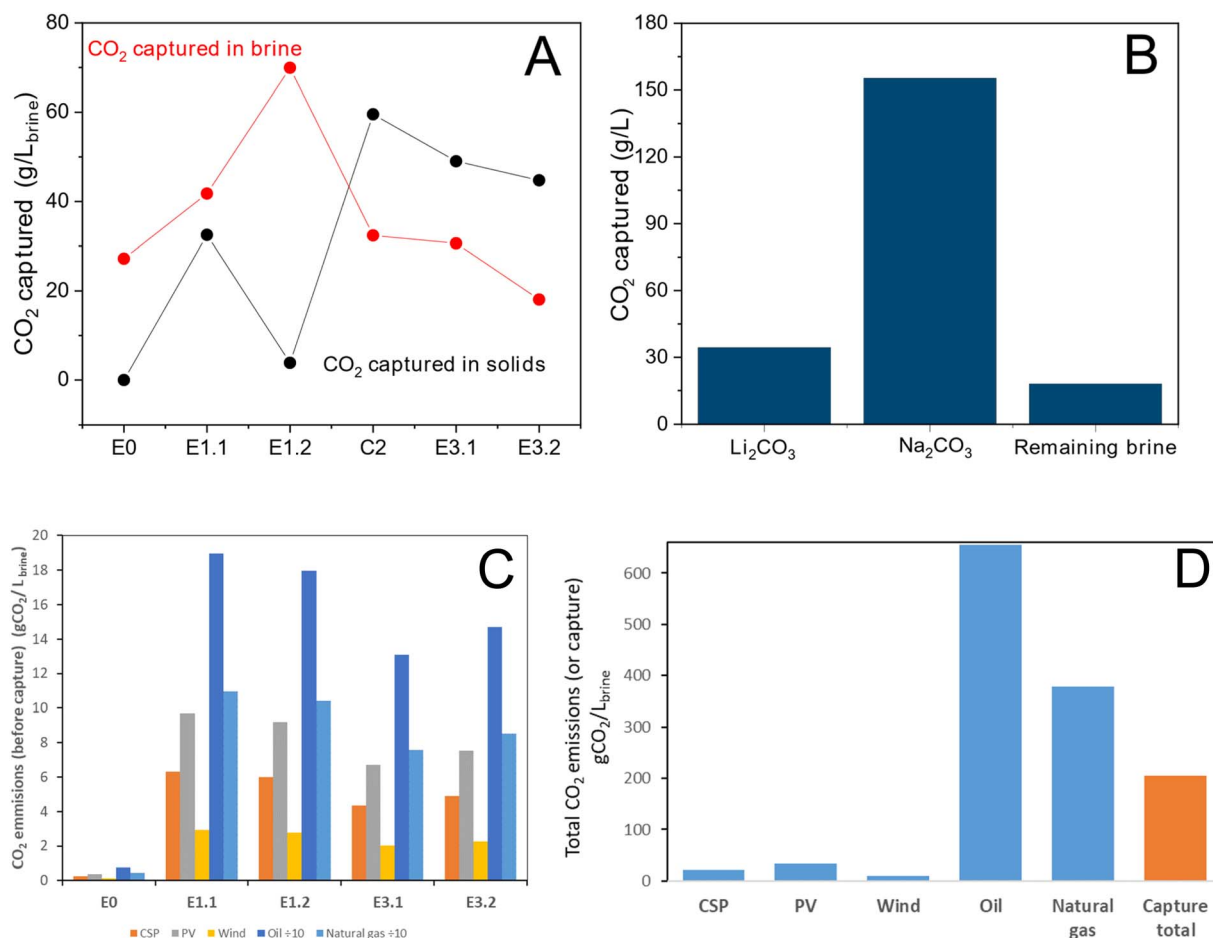**Fig. 7** Energy consumption for electrolytic steps.

Fig. 8 (A) CO_2 captured in different processing steps in brines and solids. (B) Cumulative CO_2 captured for the different solids and remaining brine (B4). (C) Estimation of CO_2 emissions for each electrolytic step for different possible energy sources. (D) Comparison of total CO_2 emissions and CO_2 capture for the overall processing strategy.

and $CO_3 2-$ concentration, the last two being easily achievable by automatic control of the CO_2 sparging rate and/or current density. The fact that a considerable fraction of CO_2 remains in the brine suggests that there are opportunities for process optimization, which opens up new possibilities both in terms of CO_2 absorption efficiency and mineralized product recovery.

Fig. 8C shows CO_2 emissions associated with different energy sources that could likely be installed close to lithium brine mines in the Lithium Triangle in South America. This region is rich in natural gas, with pipelines at relatively short distances from where extensions could be easily constructed.[30,40] The other non-renewable energy source would be oil.[40] In the absence of carbon capture and storage technology, natural gas has been associated with lower emissions than oil (Table 3). There are also ample solar and wind resources, with already installed infrastructure,[41,42] which explain our choices of renewable energy options. As expected, emissions associated with electricity production from oil and natural gas are the largest. Production from oil emits 1.73 times more CO_2 than production from natural gas, while both options emit over one order of magnitude more CO_2 than all other 3 renewable sources considered. Fig. 8D shows a comparison of the total emissions (all 5 electrolytic steps) *vs.* the total capture capacity of the

6-steps technology. If either of the 3 renewable energy options was chosen, this proposal could be classified as carbon negative, considering that a net capture (total capture minus emissions) of 172.3, 184.0 and 195.7 g_{CO_2} L_{brine}^{-1} is the balance for photovoltaics, concentrating solar power and wind, respectively. Conversely, the technology would still be carbon positive if either natural gas or oil is used.

4. Conclusions

Herein, a new strategy has been developed to promote a more sustainable lithium production from brines. The processing starts with electrolytic brine polishing. The lithium carbonation process is promoted *via* CO_2 absorption and conversion to carbonate anions in the highly alkaline brine. Alkalinity is produced *via* a continuous electrolytic process. These are zero-chemical treatments, as opposed to the current technology that requires lime (CaO) and soda ash (Na_2CO_3) to remove divalent cations and crystallize Li_2CO_3. The chemical input is replaced here by CO_2 absorption and electricity. 78% of the original Li^+ content was recovered during the two electrolytic processes coupled to CO_2 absorption as an impure Li_2CO_3 primary solid. A further 11% of the original Li^+ content was

recovered as a solid that was composed mostly of Na_2CO_3, but for which a recovery strategy could be sought.

Beyond Li_2CO_3 recovery, a chemical step was implemented to take advantage of the high brine pH to secure larger CO_2 absorption. In the absence of water reduction at the cathode, the pH dropped after a few minutes of CO_2 absorption and Na_2CO_3 crystallization. Thus, two new electrolytic steps were introduced to increase the amount of solid product formation and CO_2 mineralization. Overall, 71.8% of the original Na^+ content was removed from the brine and recovered mostly as Na_2CO_3. All tests performed here were carried out on real samples, pumped from South American lithium-rich brine deposits and pre-processed by an active lithium mining company. The nature of the tested samples further validates the proposed technology due to the high brine complexity.

In this work, focus was made on the production of solid products and the maximization of CO_2 absorption A total of 205.8 g_{CO_2} L_{brine}^{-1} were absorbed in both brine and solids. Out of that amount, 189.7 g_{CO_2} L_{brine}^{-1} are considered to have been permanently stored in highly stable mineralized products: Li_2CO_3 and Na_2CO_3. CO_2 mineralization at ambient pressure and temperature in highly saline brines is still a field much to be explored. A large amount of work remains in terms of operative costs, where there is yet a lot of room for improvement. The lithium carbonation steps deliver a concentrated pulse of CO_2 storage in brines, but the contribution to CO_2 mineralization is minimal as compared to accumulation in Na_2CO_3. In contrast, the sodium-dominated steps achieve high-yield mineralization in the last steps while permitting passive CO_2 dissolution in brines.

Author contributions

NCZ: investigation, data curation, formal analysis. WRT: conceptualization, data curation, formal analysis, investigation, methodology, writing – original draft, funding acquisition. VF: conceptualization, methodology, formal analysis, writing – original draft, writing – review & editing, funding acquisition.

Conflicts of interest

There are no conflicts of interest to declare.

Data availability

The data supporting this article have been included as part of the SI. No personal software code was used and no new crystallographic data were generated.

Current and potential plots for electrolytic steps; picture of the experimental setup used for all electrochemical experiments; anion exchange membrane specifications; tables with quantitative compositions of all solids; and SEM micrographs for analytical grade commercial samples of NaCl and $NaHCO_3$. See DOI: https://doi.org/10.1039/d5su00552c.

References

1 UNITED NATIONS, Department of Economic and Social Affairs Sustainable Development, *The 17 Goals*, https://sdgs.un.org/goals.

2 R. Sharifian, R. M. Wagterveld, I. A. Digdaya, C. Xiang and D. A. Vermaas, Electrochemical carbon dioxide capture to close the carbon cycle, *Energy Environ. Sci.*, 2021, **14**, 781–814.

3 M. Rahimi, A. Khurram, T. A. Hatton and B. Gallant, Electrochemical carbon capture processes for mitigation of CO_2 emissions, *Chem. Soc. Rev.*, 2022, **51**, 8676–8695.

4 P. Dellicompagni, L. Saravia, M. Altamirano and J. Franco, Simulation and testing of a solar reciprocating steam engine, *Energy*, 2018, **151**, 662–674.

5 H. Mohammadpour, K. Y. Cheng, A. Pivrikas and G. Ho, A review of biogas upgrading technologies: key emphasis on electrochemical systems, *Water Sci. Technol.*, 2024, **91**, 93–116.

6 J. E. Chae, J. Choi, D. Lee, S. Lee and S. Kim, Development of anion exchange membrane-based electrochemical CO2 separation cells for direct air capture, *J. Ind. Eng. Chem.*, 2025, **145**, 543–550.

7 T. N.-D. Cao, *et al.*, Unraveling the Potential of Electrochemical pH-Swing Processes for Carbon Dioxide Capture and Utilization, *Ind. Eng. Chem. Res.*, 2023, **62**, 20979–20995.

8 Q. Wang, *et al.*, Advances and Challenges in Membrane-Based Electrochemical Reactors for CO2 Capture: A Mini-Review, *Ind. Eng. Chem. Res.*, 2024, **63**, 22221–22231.

9 M. Lee, S. Saad and Y. Park, Simultaneous NaCl solution electrolysis and CO2 conversion for efficient and selective production of NaHCO3, *J. Water Process Eng.*, 2024, **66**, 105933.

10 Y. Mao, *et al.*, Theoretical and experimental validation of an electrochemical-mediated integrated system for CO2 capture and compression, *Energy Convers. Manag.*, 2025, **325**, 119377.

11 M. Shi, *et al.*, Carbon capture via electrochemically mediated alkaline absorption: lab-scale continuous operation, *J. Clean. Prod.*, 2024, **476**, 143767.

12 A. Ozden, CO2 Capture via Electrochemical pH-Mediated Systems, *ACS Energy Lett.*, 2025, **10**, 1550–1576.

13 E. Yeo, H. Shin, T. Kim, S. Kim and J. S. Kang, Electrochemically driven capacitive CO2 capture technologies, *J. Environ. Chem. Eng.*, 2025, **13**, 116092.

14 R. L. Putri, D. N. S. Werastuti, N. W. Rustiarini, A. Sutoto, E. Wahyono, B. Wardono, A. Zulham, A. Lukas, R. D. Goenawan, S. Anita, I. K. Ardana, I. N. Normal,

M. Daniel, L. Yuniarti, K. Supriadi and D. A. Vayed, Assessing the role of carbon taxes in driving low-carbon transformations: a comparative analysis of implementation policies, *Int. J. Sustain. Dev. Plan.*, 2024, **19**, 1171–1180.

15 J. Wang, Y. Zhou and F. L. Cooke, Low-carbon economy and policy implications: a systematic review and bibliometric analysis, *Environ. Sci. Pollut. Res.*, 2022, **29**, 65432–65451.

16 F. J. Millero, The thermodynamics of the carbonate system in seawater, *Geochim. Cosmochim. Acta*, 1979, **43**, 1651–1661.

17 A. G. Dickson and J. P. Riley, The estimation of acid dissociation constants in seawater media from potentionmetric titrations with strong base. I. The ionic product of water — Kw, *Mar. Chem.*, 1979, **7**, 89–99.

18 K. G. Schulz, U. Riebesell, B. Rost, S. Thoms and R. E. Zeebe, Determination of the rate constants for the carbon dioxide to bicarbonate inter-conversion in pH-buffered seawater systems, *Mar. Chem.*, 2006, **100**, 53–65.

19 N. Karo, G. Itov, O. Mayraz and C. Vogt, Carbon dioxide sequestration through mineralization from seawater: The interplay of alkalinity, pH, and dissolved inorganic carbon, *Chem. Eng. J.*, 2024, **500**, 156380.

20 T. L. Biel-Nielsen, *et al.*, Electrochemistry-Based CO2 Removal Technologies, *ChemSusChem*, 2023, **16**, e202202345.

21 D. He, X. Ma, H. Zhou, Y. Zhang and Y. Wu, Continuous conversion of flue gas into syngas by a bipolar membrane-integrated single-cell cyclic system, *Joule*, 2025, **9**, 101806.

22 S. Khan, *et al.*, Geomechanical modeling of CO2 sequestration: a review focused on CO2 injection and monitoring, *J. Environ. Chem. Eng.*, 2024, **12**, 112847.

23 H. Liu, H. Lu and H. Hu, CO2 capture and mineral storage: state of the art and future challenges, *Renew. Sustain. Energy Rev.*, 2024, **189**, 113908.

24 A. Sanna, M. Uibu, G. Caramanna, R. Kuusik and M. M. Maroto-Valer, A review of mineral carbonation technologies to sequester CO2, *Chem. Soc. Rev.*, 2014, **43**, 8049–8080.

25 S. Ó. Snæbjörnsdóttir, *et al.*, Carbon dioxide storage through mineral carbonation, *Nat. Rev. Earth Environ.*, 2020, **1**, 90–102.

26 M. Sibhat, *et al.*, Advancement in sodium carbonation pathways for sustainable carbon capture and utilization: a review, *Results Eng.*, 2024, **23**, 102536.

27 M. L. Vera, W. R. Torres, C. I. Galli, A. Chagnes and V. Flexer, Environmental impact of direct lithium extraction from brines, *Nat. Rev. Earth Environ.*, 2023, **4**, 149–165.

28 V. Flexer, C. F. Baspineiro and C. I. Galli, Lithium recovery from brines: a vital raw material for green energies with a potential environmental impact in its mining and processing, *Sci. Total Environ.*, 2018, **639**, 1188–1204.

29 D. E. Garrett, Handbook of Lithium and Natural Calcium Chloride, *Handbook of Lithium and Natural Calcium Chloride*, 2004, DOI: **10.1016/B978-0-12-276152-2.X5035-X**.

30 P. Dellicompagni, J. Franco and V. Flexer, CO2 Emission Reduction by Integrating Concentrating Solar Power into Lithium Mining, *Energy Fuels*, 2021, **35**, 15879–15893.

31 *CRC Handbook of Chemistry and Physics*, ed. W. M. Haynes, CRC Press, 97th edn, 2016.

32 J. Desloover, A. Abate Woldeyohannis, W. Verstraete, N. Boon and K. Rabaey, Electrochemical Resource Recovery from Digestate to Prevent Ammonia Toxicity during Anaerobic Digestion, *Environ. Sci. Technol.*, 2012, **46**, 12209–12216.

33 W. R. Torres, N. C. Zeballos and V. Flexer, Effect of [Na+]/[Li+] concentration ratios in brines on lithium carbonate production through membrane electrolysis, *Faraday Discuss.*, 2023, **247**, 101–124.

34 National Renewable Energy Laboratory, *Life Cycle Greenhouse Gas Emissions from Electricity Generation: Update*, **https://www.nrel.gov/analysis/life-cycle-assessment**.

35 M. Li, *et al.*, The state of the art of carbonation technology in geotechnical engineering: a comprehensive review, *Renew. Sustain. Energy Rev.*, 2023, **171**, 112986.

36 P. Ndlovu, *et al.*, Carbon dioxide utilization in mineral processing, *J. CO2 Util.*, 2025, **94**, 103063.

37 P. Turek and W. Gnot, Precipitation of Magnesium Hydroxide from Brine, *Ind. Eng. Chem. Res.*, 1995, **34**, 244–250.

38 A. A. Pilarska, Ł. Klapiszewski and T. Jesionowski, Recent development in the synthesis, modification and application of Mg(OH)2 and MgO: a review, *Powder Technol.*, 2017, **319**, 373–407.

39 D. Pletcher and F. C. Walsh, *Industrial Electrochemistry*, Springer Science & Business Media, 2012.

40 International Energy Agency, Argentina, **https://www.iea.org/countries/argentina**.

41 A. M. Oyarzún-Aravena, J. Chen, G. Brownbridge, J. Akroyd and M. Kraft, An analysis of renewable energy resources and options for the energy transition in Chile, *Appl. Energy*, 2025, **381**, 125107.

42 J. A. Bragagnolo, K. Taretto and C. Navntoft, Solar Energy in Argentina, *Solar*, 2022, **2**, 120–140.